IN-02

8130

p. 13

NASA Technical Memorandum   107567

THREE-DIMENSIONAL TIME-MARCHING AEROELASTIC ANALYSES USING AN UNSTRUCTURED-GRID EULER METHOD

RUSS D. RAUSCH
JOHN T. BATINA
HENRY T. Y. YANG

MARCH 1992

NASA

(NASA-TM-107567)   THREE-DIMENSIONAL
TIME-MARCHING AEROELASTIC ANALYSES USING AN
UNSTRUCTURED-GRID EULER METHOD   (NASA)   13 p
CSCL 01A

N92-23116

Unclas
G3/02   0085180

THREE-DIMENSIONAL TIME-MARCHING AEROELASTIC
ANALYSES USING AN UNSTRUCTURED-GRID EULER METHOD

Russ D. Rausch[*]
Purdue University
West Lafayette, Indiana 47907

John T. Batina[†]
NASA Langley Research Center
Hampton, Virginia 23665–5225

Henry T. Y. Yang[‡]
Purdue University
West Lafayette, Indiana 47907

Abstract

Modifications to a three-dimensional, implicit, upwind, unstructured-grid Euler code for aeroelastic analysis of complete aircraft configurations are described. The modifications involve the addition of the structural equations of motion for their simultaneous time integration with the governing flow equations. The paper presents a detailed description of the time-marching aeroelastic procedure and presents comparisons with experimental data to provide an assessment of the capability. Flutter results are shown for an isolated 45° swept-back wing and a supersonic transport configuration with a fuselage, clipped delta wing, and two identical rearward-mounted nacelles. Comparisons between computed and experimental flutter characteristics show good agreement, giving confidence in the accuracy of the aeroelastic capability that was developed.

Introduction

In recent years, there has been increased interest in the development of aeroelastic analysis methods involving computational fluid dynamics techniques.[1] This work in the area of computational aeroelasticity has focused on developing finite-difference codes for the solution of the transonic small-disturbance[2,3] and full potential equations,[4,5] although a growing effort is underway for the solution of the Euler and Navier-Stokes equations.[6-17] For example, Bendiksen and Kousen[6] presented transonic flutter results for two-degree-of-freedom (plunging and pitching) airfoils by simultaneously integrating the structural equations of motion and the two-dimensional unsteady Euler equations. The Euler equations were discretized in space using a finite-volume method on a moving mesh and integrated using a Runge-Kutta time-stepping scheme. The instantaneous mesh was taken to be a superposition of meshes corresponding to rigid plunging and pitching of the airfoil. In a following study, Kousen and Bendiksen[7] applied their method of Ref. 6 to investigate the nonlinear aeroelastic behavior of two-degree-of-freedom airfoils at transonic speeds and showed that transonic flutter instabilities led to stable limit-cycle oscillations involving very large amplitudes. Most recently, Bendiksen[8] presented an alternative approach to the integration of the structural equations of motion and the fluid flow equations. Wu, Kaza, and Sankar[9] integrated in time, the unsteady compressible Navier-Stokes equations for airfoils undergoing one- and two-degree-of-freedom aeroelastic motions. In Ref. 9, flutter characteristics of airfoils at high angles of attack including cases with stall flutter, were investigated. The method of Ref. 9 also has been applied by Reddy, Srivastava, and Kaza[10] to study the effects of rotational flow, viscosity, thickness, and shape on the transonic flutter dip phenomena. The study concluded that the influence of these effects on flutter, for the cases considered, was small near the minimum of the flutter dip, but may be large away from the dip. Guruswamy[11-14] demonstrated simultaneous time integration of the three-dimensional Euler and Navier-Stokes equations along with the structural equations of motion. The inviscid capability first was demonstrated in a time-marching flutter analysis performed for a rectangular wing with a parabolic-arc airfoil section, and the viscous capability was demonstrated later for an aeroelastic deformation of a blended wing body to study shock-vortex interaction. Finally, Robinson, Batina, and Yang[15] presented Euler aeroelastic results for a 45° swept-back wing using a deforming mesh capability. A common feature of the above

computational aeroelastic methods is that all involved algorithms that required a structured computational grid.

As an alternative to structured grid methods, some recent efforts in computational fluid dynamics are directed toward solving the governing flow equations using unstructured grids.[16-28] These grids typically are constructed from triangles in two dimensions, and they consist of an assemblage of tetrahedra in three dimensions. One benefit of using these geometric shapes is that they may be oriented easily to conform to the geometry being considered, making it possible to represent accurately complicated shapes such as multi-element airfoils in two dimensions or complete aircraft configurations in three dimensions. Application of the unstructured grid methodology has been demonstrated for multi-element airfoils[18, 19] and complete aircraft configurations.[20, 21] Another benefit of the unstructured grid methodology is that the grid data structure simplifies mesh refinement in regions of high-flow gradients to resolve the physics of the flow more accurately. These adaptive grid methods have been demonstrated for steady and unsteady flows in two dimensions[22-25] and for complex geometries in three dimensions.[26, 27] A disadvantage, however, of the unstructured grid methodology is the computational overhead of the indirect addressing used to maintain the grid data structure. For example, the computational work, for steady-state solutions obtained using unstructured grid algorithms, has been shown to be 2 to 5 times more expensive than that required to obtain solutions on a structured grid with the same number of cells.[29]

Since there are a number of benefits in using unstructured grid methods, it is appropriate to develop computer codes for transonic aeroelastic analysis of complete aircraft configurations. As a first step, an assessment of the applicability of the unstructured grid methodology for the aeroelastic analysis of airfoils was developed and reported by the present authors in Ref. 16. Comparisons were made with solutions obtained using a structured grid code to determine the accuracy of the unstructured grid methodology. The unstructured grid capability included a deforming mesh algorithm to allow the grid to conform to the instantaneous position of the moving or deforming airfoil under consideration. The algorithm is quite general and necessary for the treatment of realistic motions encountered during an aeroelastic calculation. The conclusion in Ref. 16 was that accurate flutter results could be computed using the unstructured grid methodology. In an independent study by Mortchelewitcz and Sens,[17] three-dimensional unsteady results were presented for a wing undergoing forced harmonic motion. In Ref. 17 comparisons of calculated unsteady pressures were made with experimental data. The capability included the implementation of transpiration boundary conditions that allowed the mesh to remain fixed for unsteady applications where the relative motion of the geometry is assumed small.

The purpose of the present study is to incorporate the aeroelastic analysis procedures of Ref. 16 into a three-

dimensional, implicit, upwind Euler scheme on unstructured deforming meshes and to assess the applicability of the unstructured grid methodology for aeroelastic analysis of complete aircraft configurations. The objectives of the research are: (1) to develop a solution algorithm for time accurate unsteady flow calculations on a deforming mesh, (2) to implement the aeroelastic analysis procedures, (3) to compute aeroelastic results for an isolated wing and for a complete aircraft configuration, and (4) to determine the accuracy of the solutions by making comparisons with available experimental data. The eventual goal is to develop a highly-accurate and efficient solution algorithm for the Euler and Navier-Stokes equations for aeroelastic analysis of complex aircraft configurations. The paper gives a brief description of the flow solver used in the current effort, a description of the deforming mesh algorithm, and the time-marching aeroelastic analysis procedures. To demonstrate the time-marching aeroelastic procedure that was implemented, flutter results are presented for an isolated 45° swept-back wing and a supersonic transport configuration with a clipped delta wing and two rearward-mounted nacelles. The authors believe that these are the first three-dimensional flutter calculations obtained using the unstructured-grid methodology. The paper also presents comparisons between computed and experimental flutter characteristics to provide an assessment of the accuracy of the capability.

Upwind-Type Euler Solution Algorithm

The Euler equations are solved using the three-dimensional upwind-type solution algorithm developed by Batina.[28] The solution algorithm of Ref. 28 was extended by Rausch[30] for time-accurate unsteady flow calculations on a deforming mesh and demonstrated for AGARD case 5, proposed by the AGARD Structures and Materials Panel.[31] The algorithm, which is a cell-centered finite-volume scheme, uses upwind differencing based on flux-vector splitting,[32] similar to upwind schemes developed for use on structured meshes. The flux-split discretization accounts for the local wave-propagation characteristics of the flow and captures shock waves sharply with at most one grid point within the shock structure. An additional advantage of using flux-splitting is that the discretization is naturally dissipative and, consequently, does not require additional artificial dissipation terms or the adjustment of free parameters to control the dissipation. However, in calculations involving a higher-order upwind scheme such as this, oscillations in the solution near shock waves are expected to occur. To eliminate these oscillations, flux limiting usually is required. In the present study, a continuously differentiable flux limiter was employed.

The Euler equations are integrated in time using an implicit time-integration scheme involving a Gauss-Seidel relaxation procedure.[28] The relaxation procedure is implemented by re-ordering the elements that make up the un-

structured mesh from upstream to downstream. The solution is obtained by sweeping two times through the mesh as dictated by stability considerations. The first sweep is performed in the direction from upstream to downstream and the second sweep is from downstream to upstream. For purely supersonic flows the second sweep is unnecessary. This relaxation scheme is stable for large time steps and thus allows the selection of the step size based on the temporal accuracy of the problem being considered, rather than on the numerical stability of the algorithm. Consequently, very large time steps may be used for rapid convergence to steady state, and an appropriate step size may be selected for unsteady cases, independent of numerical stability issues.

Deforming Mesh Algorithm

A deforming mesh algorithm is used to move the mesh for unsteady calculations where the geometry deforms. The method, as developed in Ref. 33, models the mesh as a spring network where each edge of each tetrahedra represents a spring with a stiffness inversely proportional to the length of that edge. In this procedure, grid points along the outer boundary of the mesh are held fixed, and the instantaneous locations of the points on the wing (inner boundary) are specified. For aeroelastic calculations, the position of the inner boundary is determined by the structural equations of motion. The locations of the interior nodes then are determined by solving the static equilibrium equations that result from a summation of forces at each node in the x, y, and z coordinate directions. The solution of the equilibrium equations is approximated by using a predictor-corrector procedure, which first predicts the new locations of the nodes by extrapolation from grids at previous time levels and then corrects these locations by using several Jacobi iterations of the static equilibrium equations. The predictor-corrector procedure is relatively efficient because of the small number of Jacobi iterations required to move the mesh.

Time-Marching Aeroelastic Analysis

In this section the aeroelastic equations of motion, the time-marching solution procedure, and the modal identification technique are described.

Aeroelastic Equations of Motion

The aeroelastic equations of motion can be written for each mode i as

$$m_i \ddot{q}_i + c_i \dot{q}_i + k_i q_i = Q_i \tag{1}$$

where q_i is the generalized displacement, m_i is the generalized mass, c_i is the generalized damping, k_i is the generalized stiffness, and Q_i is the generalized force computed by integrating the pressure weighted by the mode shapes. These

equations of motion are derived by assuming that the deformation of the body under consideration can be described by a separation of variables involving the summation of free vibration modes weighted by generalized displacements. The implementation of the equations of motion are slightly different than that of Refs. 3, 15, and 16. In this development the generalized aerodynamic forces include modal deflections in all three coordinate directions whereas previous implementations involved deflections only in the vertical direction. It is noted, however, that the results present herein involve deflections only in the vertical direction.

Time-Marching Solution

The solution procedure for integrating Eq. (1) is similar to that described by Edwards et al.[34, 35] A similar formulation is implemented in the present study for multiple degrees of freedom. Here the linear state equations are written as

$$\dot{x}_i = Ax_i + Bu_i \tag{2}$$

where A and B are coefficient matrices that result from the change of variables $x_i = [q_i \; \dot{q}_i]^T$, and u_i is the nondimensional representation of the generalized force Q_i. Equation (2) is integrated in time using the modified state-transition matrix structural integrator[35] implemented as a predictor-corrector procedure. The prediction for x_i^{n+1}, $\tilde{x}_i^{n+1}$, is given by

$$\tilde{x}_i^{n+1} = \Phi x_i^n + \Theta B \left(3u_i^n + u_i^{n-1}\right)/2 \tag{3}$$

where Φ is the state-transition matrix, and Θ is the integral of the state-transition matrix from time step n to $n + 1$. Then, $\tilde{x}_i^{n+1}$ is used to compute the flow field and evaluate the nondimensional generalized force $\tilde{u}_i^{n+1}$. These values then are used in the corrector step to determine x_i^{n+1}, given by

$$x_i^{n+1} = \Phi x_i^n + \Theta B \left(\tilde{u}_i^{n+1} + u_i^n\right)/2 \tag{4}$$

Modal Identification Technique

Damping and frequency characteristics of the aeroelastic responses are estimated from the response curves by using the modal identification technique of Bennett and Desmarais.[36] The modal estimates are determined by a least squares curve fit of the responses of the form

$$q_i(T) = a_0 + \sum_{j=1}^{m} e^{\sigma_j T} [a_j cos(\omega_j T) + b_j sin(\omega_j T)] \tag{5}$$

$$i = 1, 2, \ldots$$
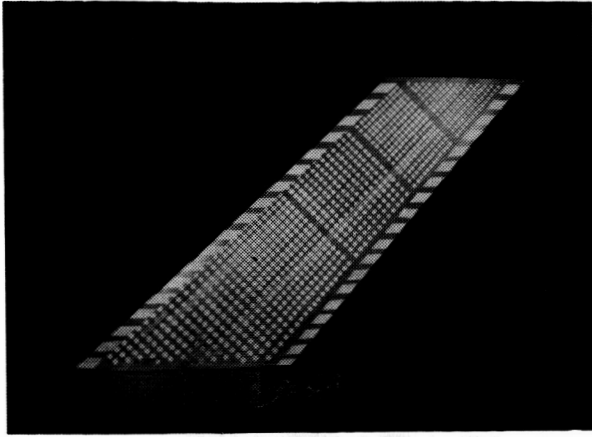
where m is the number of modes.
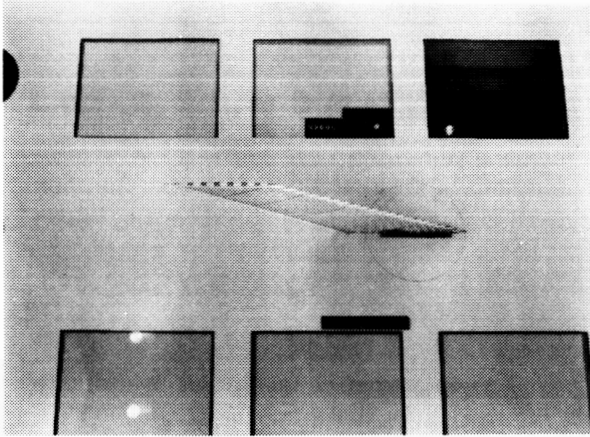
Fig. 1 Planview of 45° swept-back wing model.

Fig. 2 45° swept-back wing model in the NASA Langley Transonic Dynamics Tunnel.

(a) Oblique projections.

(b) Deflection contour lines.

Fig. 3 Natural vibration modes of the 45° swept-back wing.

Results and Discussion

Flutter results are presented in this section for a 45° swept-back wing and for a supersonic transport configuration with a clipped delta wing and two rearward-mounted nacelles. The results are used to assess the time-marching aeroelastic capability. The accuracy of the results is determined by making comparisons with available experimental data.

45° Swept-back Wing

To assess the unstructured-grid code for three-dimensional aeroelastic applications, a simple well-defined wing was selected as a first step towards performing aeroelastic analyses for complete aircraft configurations. The wing that was analyzed was a half-span wind-tunnel-wall-mounted model that has a quarter-chord sweep angle of 45°, a panel aspect ratio of 1.65, and a taper ratio of 0.66.[37] The wing is an AGARD standard aeroelastic configuration
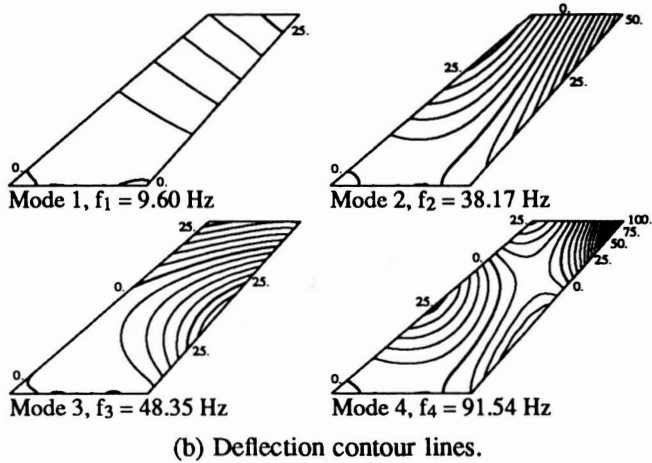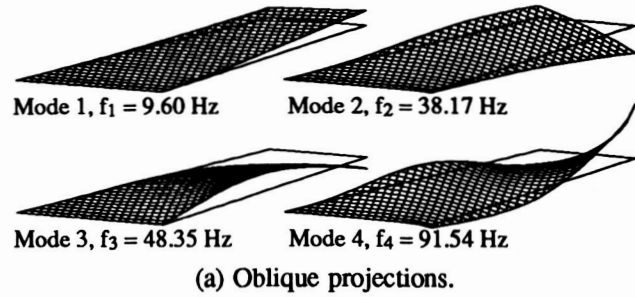
which was tested in the Transonic Dynamics Tunnel (TDT) at NASA Langley Research Center. A planview of the wing is shown in Fig. 1. The wing has a NACA 65A004 airfoil section and was constructed of laminated mahogany and hence was essentially homogeneous. In order to obtain flutter for a wide range of flow Mach numbers and densities in the TDT, holes were drilled through the wing to reduce its stiffness. To maintain the aerodynamic shape of the wing, the holes were filled with a rigid foam plastic. A photograph of the wing mounted in the TDT is shown in Fig. 2.

The wing is modeled structurally using the first four natural vibration modes which are illustrated in Figs. 3(a) and (b). Figure 3(a) shows oblique projections of the natural modes, while Fig. 3(b) shows the corresponding deflection contours. These modes, which are numbered 1 through 4, represent first bending, first torsion, second bending, and second torsion, respectively, as determined by a finite element analysis. The modes have natural frequencies which range from 9.6 Hz for the first bending mode to 91.54 Hz for the second torsion mode.

The 45° swept-back wing was modeled using an unstructured mesh generated by an advancing front method that is part of the VGRID3D[38] software package. The computational mesh used in the calculations extends two wing semispans from the symmetry plane in the span direction. Also, the mesh extends ten root chordlengths above/below and upstream/downstream of the wing surface to rectangular outer boundaries. The meshes on the upper and lower surfaces of the wing are shown in Fig. 4 which indicates that
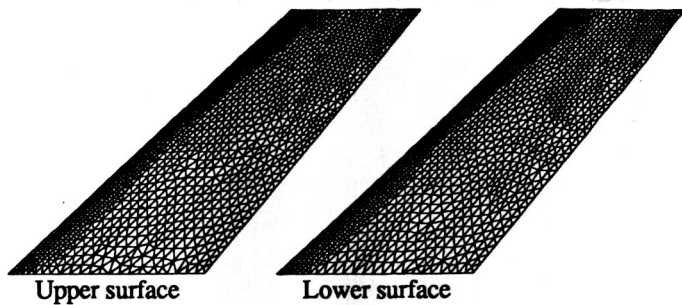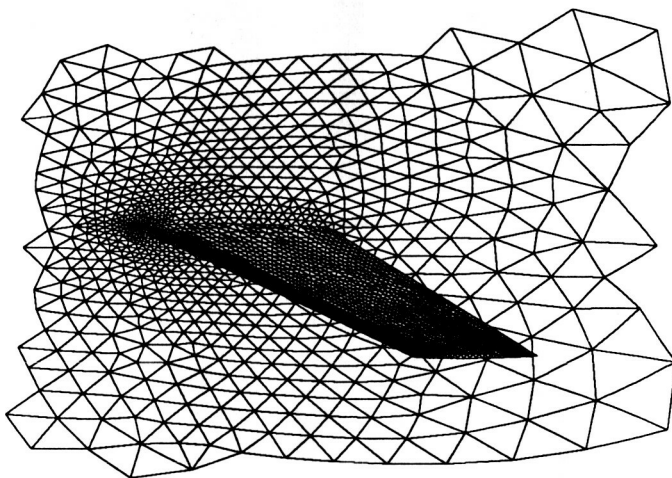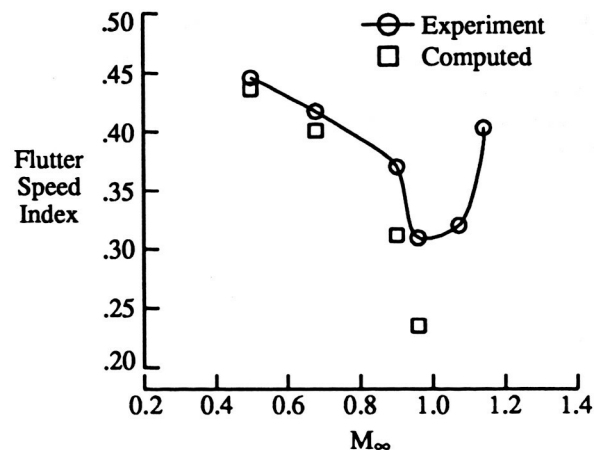
4

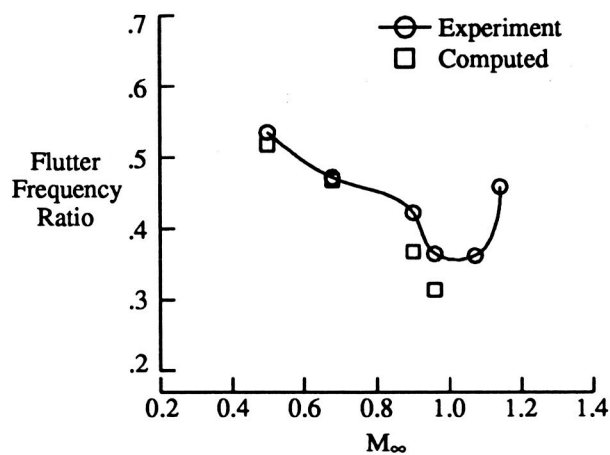Fig. 4 Surface mesh for the 45° swept-back wing.

Fig. 5 Partial view of the surface mesh for the symmetry plane and the 45° swept-back wing.

(a) Flutter speed index.

(b) Flutter frequency ratio.

Fig. 6 Comparisons of Euler flutter predictions with experimental data for the 45° swept-back wing.

cells have been clustered near the leading edge of the wing. The leading edge is a region of large flow gradients, and the clustered cells produce a more accurate calculation of the leading edge surface pressure. Figure 5 shows a partial view of the plane of symmetry and the wing. In this figure the mesh along the symmetry plane shows how the cells are stretched away from the wing. The complete mesh for the wing contains 129,746 tetrahedra and 23,727 nodes.

Flutter characteristics were calculated for comparison with measured values of the flutter speed index and the nondimensional flutter frequency at free stream Mach numbers, M_∞, of 0.499, 0.678, 0.901, and 0.960 at zero degrees angle of attack. The calculation of each flutter point was started by obtaining a steady-rigid solution at the above flow conditions. Typically, the next step is to compute a static-aeroelastic solution, however, for these steady-state flow conditions the wing does not deflect statically since the wing is symmetric and at zero degrees angle of attack. Therefore, once the steady-rigid solution was obtained for each Mach number, a dynamic-aeroelastic calculation was started by perturbing the first two structural modes with initial velocity conditions. To bracket the flutter point, time-marching calculations were performed for several values of dynamic pressure, Q, nondimensionalized by the measured flutter dynamic pressure, Q_{exp}, including Q/Q_{exp} of 0.7, 0.8, 0.9, 1.0, and 1.1.

The aeroelastic responses that result are analyzed using the method of Ref. 36 for their damping and frequency components. These components along with their corresponding value of dynamic pressure are interpolated to zero damping of the dominant flutter mode to obtain the flutter point. Figure 6 shows comparisons of computed flutter characteristics with experimental data. Plots of flutter speed index and nondimensional flutter frequency as a function of freestream Mach number, are shown in Figs. 6(a) and 6(b), respectively. The experimental flutter data defines a typical transonic flutter "dip" with the bottom near $M_\infty = 1.0$ for this case. The bottom of the dip in flutter speed index (Fig. 6(a)) was defined by the approach to the $M_\infty = 1.072$ flutter point during the wind-tunnel operation. Results from the Euler code are presented at the values of M_∞ at which the flutter data was measured. In the Mach number range considered in this study ($0.499 \leq M_\infty \leq 0.96$), a conservative flutter speed was computed at all four Mach numbers in comparison with the experimental data. In general

the computed results agree well with experimental data at $M_\infty = 0.499$ and 0.678 in flutter speed index and in frequency ratio. Near the transonic flutter dip, however, the computed results deviate from the data for the flutter speed index but show fair agreement in flutter frequency ratio. The flutter results presented above are believed by the authors to be the first three-dimensional flutter results obtained using the unstructured-grid methodology.

Supersonic Transport Configuration

To assess the code for complete aircraft aeroelastic applications a calculation was performed for a complex configuration. This configuration represents an increase in complexity from that of the 45° swept-back wing from the standpoint of the increased complexity of the geometry and the natural vibration modes. The configuration analyzed was a half-span model of an early supersonic transport (SST) configuration that was tested in heavy gas in the NASA Langley TDT.[39, 40] This configuration consisted of a rigid fuselage and a flexible clipped delta wing with two rearward-mounted simulated engine nacelles. A view of the model mounted in the TDT is presented in Fig. 7. The wing that is analyzed in this paper is that denoted as Wing C in Ref. 39. The wing has a leading-edge sweep angle of 50.5°, a panel aspect ratio
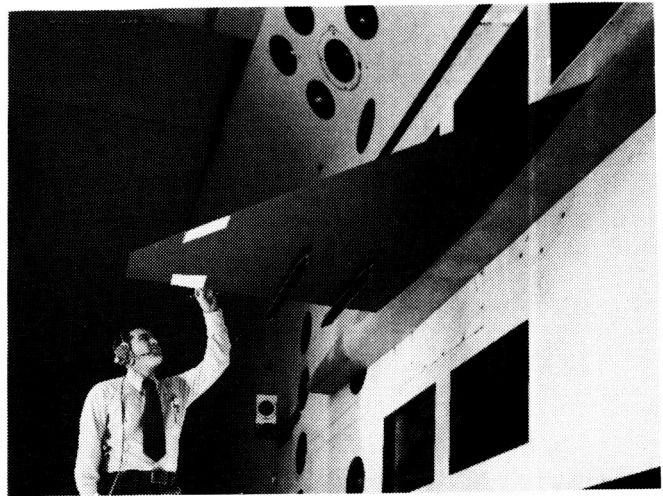

Fig. 7 Supersonic transport model with clipped delta wing in the NASA Langley Transonic Dynamics Tunnel.

of 1.24, and a taper ratio of 0.142. The airfoil section is a circular arc with a maximum thickness-to-chord ratio of 0.03. The wing was constructed of a load-carrying aluminum-alloy plate structure with cutouts, chemically milled to simulate a beam structure and was covered with balsa wood which was contoured to the desired airfoil shape. The wing was clamped to a relatively rigid mounting block which was at-

Mode 1, f_1=7.8 Hz Mode 2, f_2=16.4 Hz Mode 3, f_3=24.1 Hz

Mode 4, f_4=25.4 Hz Mode 5, f_5=38.2 Hz Mode 6, f_6=43.3 Hz

Mode 7, f_7=45.9 Hz Mode 8, f_8=48.2 Hz Mode 9, f_9=58.1 Hz
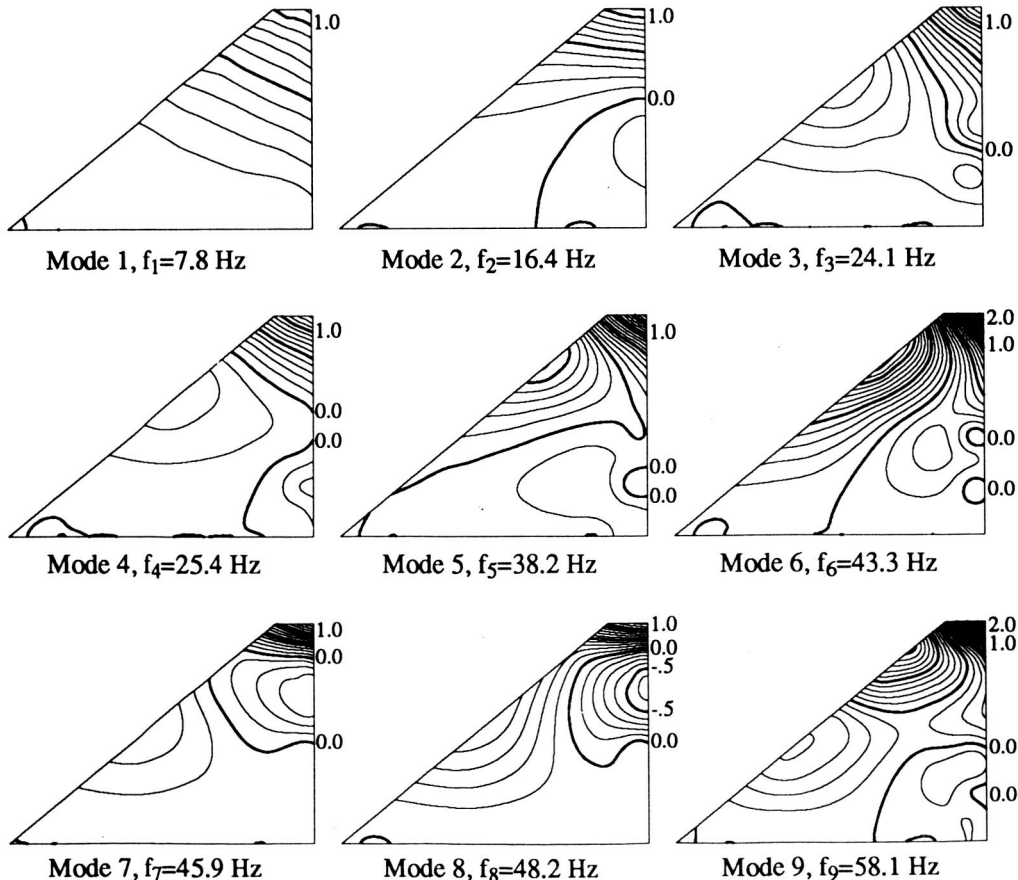
Fig. 8 Deflection contours of the natural vibration modes for the clipped delta wing of the supersonic transport model.

6

tached to a turntable on the tunnel wall. This mounting arrangement isolated the wing vibrations to the turntable and prevented structural interaction between the wing and fuselage. The model also had two identical slender under-wing bodies to simulate engine nacelles. Each nacelle consisted of a cylindrical centerbody with an ogive nose section and a conical tail fairing. The total mass of the nacelles was about the same as the total mass of the wing. The fuselage fairing was a half body of revolution that was extended from the tunnel-wall to ensure that the wing root was outside the tunnel-wall boundary layer (Fig. 7).

Nine natural vibration modes and their associated generalized masses were measured.[39] Deflection contours of these wing modes are shown in Fig. 8. These modes have natural frequencies that range from 7.8 Hz for mode 1 to 58.1 Hz for mode 9. The nacelle masses have a large effect on the mode shapes, as shown in Fig. 8, particularly in the inboard region of the wing.

The SST configuration also was modeled using the VGRID3D mesh generation package. The computational mesh extends two wing semispans from the symmetry plane in the span direction. Also, the mesh extends ten root chordlengths above/below and upstream/downstream of the wing surface to rectangular outer boundaries. The top, bottom, and side views of the surface mesh of the configuration are shown in Fig. 9. The upper and lower views of the surface mesh show that cells have been clustered near the wing tip and around the nacelles. The side view shows that

the wing is placed below the centerline of the fuselage. The complete mesh for the supersonic transport contains 323,818 tetrahedra and 59,429 nodes.

The measured natural vibration mode shapes are interpolated to the surface mesh of the configuration of Fig. 9. The interpolated mode shapes of the configuration are shown in Fig. 10 along with the corresponding natural frequencies. Figure 10 illustrates the relative vertical motion of the clipped delta wing and nacelles with respect to the rigid fuselage. Similar to the model in the wind-tunnel test, the fuselage was rigid as shown in Fig. 10. It should be noted, however, that the time-marching aeroelastic capability allows for general motion of the complete configuration and is *not* restricted to simple wing deflections.

A calculation was performed for the SST configuration at $M_\infty = 0.907$ and zero degrees angle of attack. The aeroelastic calculation was performed by first obtaining a steady-rigid solution at these flow conditions. Next a static-aeroelastic solution, during which the wing was allowed to deform due to the aerodynamic loads caused by the nonsymmetric geometry, was computed. To allow rapid convergence of the wing to its static deformed shape and to prevent the wing from oscillating, structural damping was added. Finally a dynamic-aeroelastic calculation was started from the static-aeroelastic solution by perturbing the first three structural modes with initial velocity conditions. Figure 11 shows the resulting generalized displacements for the first three structural modes, where a value of dynamic
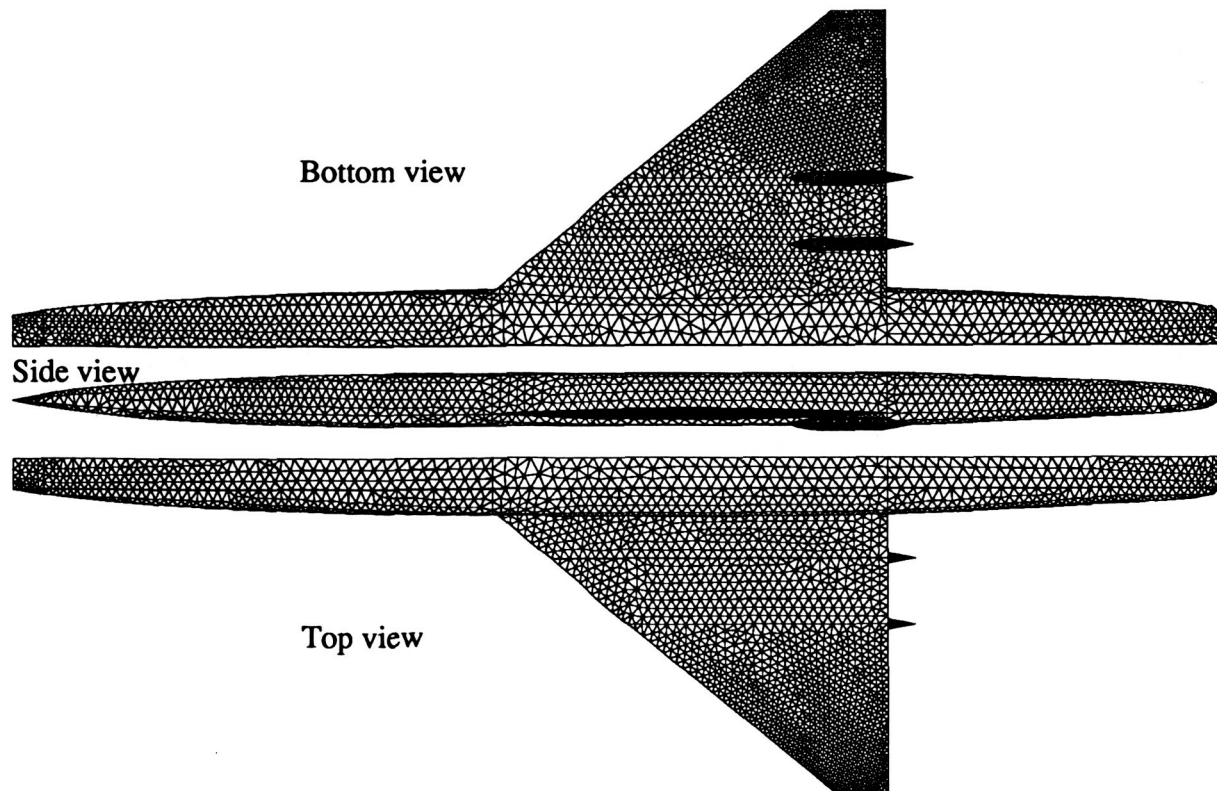

Fig. 9 Surface mesh of the supersonic transport configuration with a clipped delta wing and two rearward-mounted nacelles.

7

Mode 1, $f_1 = 7.8$ Hz   Mode 2, $f_2 = 16.4$ Hz   Mode 3, $f_3 = 24.1$ Hz

Mode 4, $f_4 = 25.4$ Hz   Mode 5, $f_5 = 38.2$ Hz   Mode 6, $f_6 = 43.3$ Hz

Mode 7, $f_7 = 45.9$ Hz   Mode 8, $f_8 = 48.2$ Hz   Mode 9, $f_9 = 58.1$ Hz
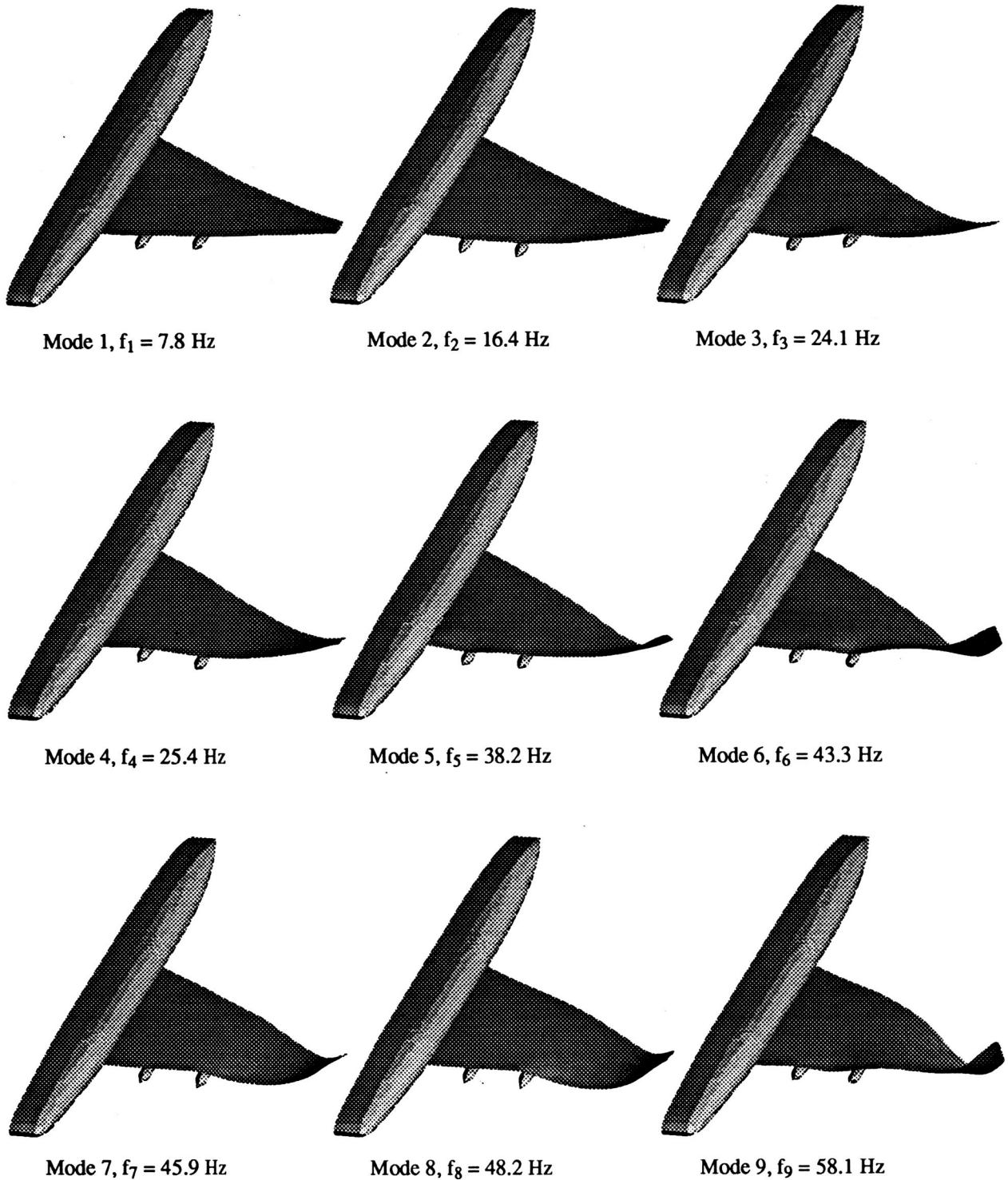
Fig. 10 Natural vibration mode shapes of the supersonic transport configuration with a clipped delta wing and two rearward-mounted nacelles.

pressure that was found experimentally to correspond to flutter was used.   The first three component modes of the second generalized displacement are shown in Fig. 12. Damping and frequency estimates of the three modes are listed in Table 1.   The near neutrally stable Mode 1 of the generalized displacement indicates the computed aeroelastic transient is near the flutter point. Therefore, the computed value of dynamic pressure is in good agreement with the value found experimentally to correspond to flutter. The calculated flutter frequency was found to be 10 Hz which compares with the experimental flutter frequency of 11 Hz.
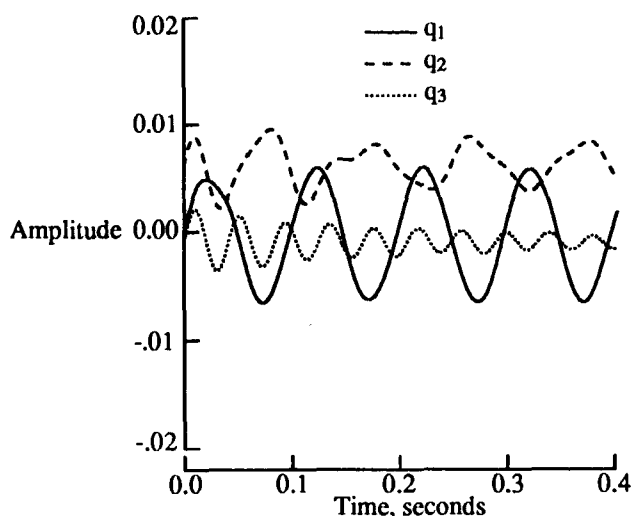
Fig. 11 Generalized displacements at $Q/Q_{exp} = 1.0$ for the supersonic transport configuration at $M_\infty = 0.907$ and zero degrees angle of attack.
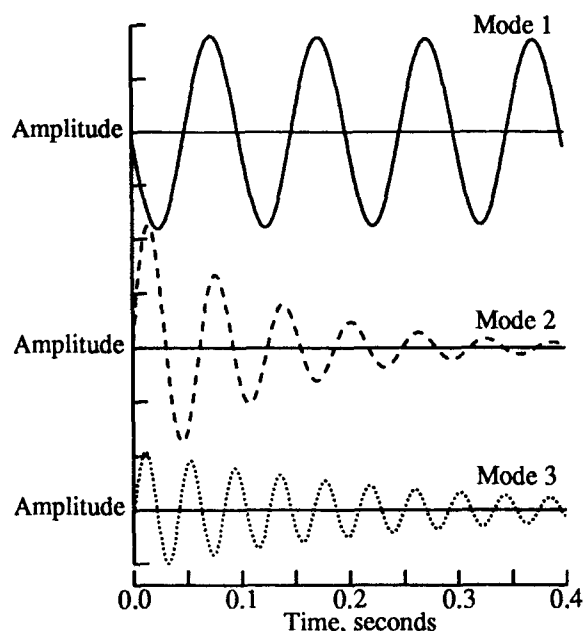

Fig. 12 First three component modes of the second generalized displacement at $Q/Q_{exp} = 1.0$ for the supersonic transport configuration at $M_\infty = 0.907$ and zero degrees angle of attack.

Concluding Remarks

Modifications to a three-dimensional, implicit, upwind Euler code based on unstructured grids for the aeroelastic analysis of complete aircraft configurations were described. The modifications involved the addition of the structural equations of motion for their simultaneous time integration with the governing flow equations. The flow solver of the Euler code, which is a cell-centered finite-volume scheme, uses upwind differencing based on flux-vector splitting and involves an implicit time-integration scheme which uses a Gauss-Seidel relaxation procedure. The code also includes a deforming mesh algorithm that is capable of moving the mesh for general aeroelastic motions of complete aircraft configurations. Flutter results were presented for an isolated 45° swept-back wing and a supersonic transport configuration with a clipped delta wing and two rearward-mounted nacelles to assess the time-marching aeroelastic procedure that was implemented. Comparisons show good agreement between computed and experimental flutter characteristics, giving confidence in the accuracy of the aeroelastic capability. The authors believe these are the first three-dimensional flutter calculations obtained using the unstructured-grid methodology.

Table 1 Component mode damping and frequencies of the aeroelastic system at $Q/Q_{exp} = 1.0$ for the supersonic transport configuration at $M_\infty = 0.907$ and zero degrees angle of attack.

Mode 1		Mode 2		Mode 3	
ζ	ω (Hz)	ζ	ω (Hz)	ζ	ω (Hz)
0.002	10.06	0.082	16.04	0.027	24.08

References

[1] Edwards, J. W., and Malone, J. B., "Current Status of Computational Methods for Transonic Unsteady Aerodynamic and Aeroelastic Applications," NASA TM 104191, Dec. 1991.

[2] Borland, C. J., and Rizzetta, D. P., "Nonlinear Transonic Flutter Analysis," AIAA Journal, vol. 20, no. 11, pp. 1606–1615, 1982.

[3] Batina, J. T., Seidel, D. A., Bland, S. R., and Bennett, R. M., "Unsteady Transonic Flow Calculations for Realistic Aircraft Configurations," Journal of Aircraft, vol. 26, no. 1, pp. 21–28, 1989.

[4] Isogai, K., and Suetsuga, K., "Numerical Simulation of Transonic Flutter of a Supercritical Wing," TR-276T, National Aerospace Laboratory, Japan, Aug. 1982.

[5] Ide, H., and Shankar, V. J., "Unsteady Full Potential Aeroelastic Computations for Flexible Configurations," AIAA Paper No. 87-1238, June 1987.

9

[6] Bendiksen, O. O., and Kousen, K. A., "Transonic Flutter Analysis Using the Euler Equations," AIAA Paper No. 87-0911, Apr. 1987.

[7] Kousen, K. A., and Bendiksen, O. O., "Nonlinear Aspects of the Transonic Aeroelastic Stability Problem," AIAA Paper No. 88-2306, Apr. 1988.

[8] Bendiksen, O. O., "A New Approach to Computational Aeroelasticity," AIAA Paper No. 91-0939, Apr. 1991.

[9] Wu, J., Kaza, K. R. V., and Sankar, L. N., "A Technique for the Prediction of Airfoil Flutter Characteristics in Separated Flow," AIAA Paper No. 87-0910, Apr. 1987.

[10] Reddy, T. S. R., Srivastava, R., and Kaza, K. R. V., "The Effects of Rotational Flow, Viscosity, Thickness, and Shape on Transonic Flutter Dip Phenomena," AIAA Paper No. 88-2348, Apr. 1988.

[11] Guruswamy, G. P., "Time-Accurate Unsteady Aerodynamic and Aeroelastic Calculations of Wings Using Euler Equations," AIAA Paper No. 88-2281, Apr. 1988.

[12] Guruswamy, G. P., "Vortical Flow Computations on Swept FlexibleWings Using Navier-Stokes Equations," AIAA Paper No. 89-1183, Apr. 1989.

[13] Guruswamy, G. P., "Navier-Stokes Computations on Swept-Tapered Wings, Including Flexibility," AIAA Paper No. 90-1152, Apr. 1990.

[14] Guruswamy, G. P., "Vortical Flow Computations on a Flexible Blended Wing-Body Configuration," AIAA Paper No. 91-1013-CP, Apr. 1991.

[15] Robinson, B. A., Batina, J. T., and Yang, H. T. Y., "Aeroelastic Analysis of Wings Using the Euler Equations with a Deforming Mesh," AIAA Paper No. 90-1032, Apr. 1990.

[16] Rausch, R. D., Batina, J. T., and Yang, H. T. Y., "Euler Flutter Analysis of Airfoils Using Unstructured Dynamic Meshes," AIAA Paper No. 89-1384, Apr. 1989.

[17] Mortchelewitcz, G. D., and Sens, A. S, "Solution of 3-D Euler Equations with Unstructured Meshes for Aeroelasticity Problems," International Forum on Aeroelasticy and Structural Dynamics 1991, June 1991.

[18] Mavriplis, D., and Jameson, A., "Multigrid Solution of the Two-Dimensional Euler Equations on Unstructured Triangular Meshes," AIAA Paper No. 87-0353, Jan. 1987.

[19] Morgan, K., Peraire, J., Thareja, R. R., and Stewart, J. R., "An Adaptive Finite Element Scheme for the Euler and Navier-Stokes Equations," AIAA Paper No. 87-1172, June 1987.

[20] Jameson, A., Baker, T. J., and Weatherill, N. P., "Calculation of Inviscid Transonic Flow Over a Complete Aircraft," AIAA Paper No. 86-0103, Jan. 1986.

[21] Peraire, J., Peiro, J., Formaggia, L., and Morgan, K., "Finite Element Euler Computations in Three Dimensions," AIAA Paper No. 88-0032, Jan. 1988.

[22] Löhner, R., and Laboratory for Computational Physics and Fluid Dynamics, "The Efficient Simulation of Strongly Unsteady Flows by the Finite Element Method," AIAA Paper No. 87-0555, Jan. 1987.

[23] Löhner, R., "An Adaptive Finite Element Solver for Transient Problems with Moving Bodies," Computers and Structures, vol. 30, pp. 303–317, 1988.

[24] Baum, J. D., and Löhner, R., "Numerical simulation of shock-elevated box interaction using an adaptive finite-element shock capturing scheme," AIAA Paper No. 89-0653, Jan. 1989.

[25] Rausch, R. D., Batina, J. T., and Yang, H. T. Y., "Spatial Adaption Procedures on Unstructured Meshes for Accurate Unsteady Aerodynamic Flow Computation," AIAA Paper No. 91-1106, Apr. 1991.

[26] Löhner, R., "Adaptive H-Refinement on 3-D Unstructured Grids for Transient Problems," AIAA Paper No. 89-0365, Jan. 1989.

[27] Löhner, R., and Baum, J. D., "Numerical Simulation of Shock Interaction with Complex Geometry Three-Dimensional Structures Using a New Adaptive H-Refinement Scheme on Unstructured Grids," AIAA Paper No. 90-0700, Jan. 1990.

[28] Batina, J. T., "Three-Dimensional Flux-Split Euler Schemes Involving Unstructured Dynamic Meshes," AIAA Paper No. 90-1649, June 1990.

[29] M. D. Salas, ed., Accuracy of Unstructured Grid Techniques Workshop, (NASA Langley Research Center, Hampton, Virginia), Jan. 17-18 1990. NASA Conference Proceedings in progress.

[30] Rausch, R. D., Time-Marching Aeroelastic and Spatial Adaptation Procedures Using an Unstructured-Grid Euler Method. PhD thesis, Purdue University, to be published.

[31] Bland, S. R., (compiler), "AGARD Two-Dimensional Aeroelastic Configurations," AGARD-AR-156, Aug. 1979.

[32] Van Leer, B., "Flux-Vector Splitting for the Euler Equations," Lecture Notes in Physics, vol. 170, pp. 507–512, 1982.

[33] Batina, J. T., "Unsteady Euler Algorithm With Unstructured Dynamic Mesh for Complex-Aircraft Aeroelastic Analysis," AIAA Paper No. 89–1189, Apr. 1989.

[34] Edwards, J. W., Bennett, R. M., Whitlow, W., Jr, and Seidel, D. A., "Time-Marching Transonic Flutter Solutions Including Angle-of-Attack Effects," Journal of Aircraft, vol. 20, no. 11, pp. 899–906, 1984.

[35] Edwards, J. W., Bennett, R. M., Whitlow, W., Jr, and Seidel, D. A., "Time-Marching Transonic Flutter Solutions Including Angle-of-Attack Effects," AIAA Paper No. 82-3685, May 1982.

[36] Bennett, R. M., and Desmarais, R. N., "Curve Fitting of Aeroelastic Transient Response Data with Exponential

Functions," In "Flutter Testing Techniques," NASA SP-415, pp. 43–58, May 1975.

[37] Yates, E. C., Jr., Land, N. S., and Foughner, J. T., Jr., "Measured and Calculated Subsonic and Transonic Flutter Characteristics of a 45° Sweptback Wing Planform in Air and in Freon-12 in the Langley Transonic Dynamics Tunnel," NASA TN D-1616, Mar. 1963.

[38] Parikh, P., Pirzadeh, S., and Löhner, R., "A Package for 3-D Unstructured Grid Generation, Finite-Element Flow Solution and Flow Field Visualization," NASA CR-182090, Sept. 1990.

[39] Sandford, M. C., Ruhlin, C. L., and Abel, I., "Transonic Flutter Study of a 50.5-Deg Cropped-Delta Wing with Two Rearward-Mounted Nacelles," NASA TN D-7544, 1974.

[40] Sandford, M. C., Abel, I., and Gray, D. L., "Development and Demonstration of a Flutter-Suppression System Using Active Controls," NASA TR R-450, Dec. 1975.

REPORT DOCUMENTATION PAGE

Public reporting burden for this collection of information is estimated to average 1 hour per response, including the time for reviewing instructions, searching existing data sources, gathering and maintaining the data needed, and completing and reviewing the collection of information. Send comments regarding this burden estimate or any other aspect of this collection of information, including suggestions for reducing this burden, to Washington Headquarters Services, Directorate for Information Operations and Reports, 1215 Jefferson Davis Highway, Suite 1204, Arlington, VA 22202-4302, and to the Office of Management and Budget, Paperwork Reduction Project (0704-0188), Washington, DC 20503.

1. AGENCY USE ONLY (Leave blank)	2. REPORT DATE March 1992	3. REPORT TYPE AND DATES COVERED Technical Memorandum

4. TITLE AND SUBTITLE
Three-Dimensional Time-Marching Aeroelastic Analyses Using an
Unstructured-Grid Euler Method

5. FUNDING NUMBERS
WU 505-63-50-12

6. AUTHOR(S) Russ D. Rausch, John T. Batina, Henry T. Y. Yang

7. PERFORMING ORGANIZATION NAME(S) AND ADDRESS(ES)
NASA Langley Research Center
Hampton, VA 23665-5225

8. PERFORMING ORGANIZATION REPORT NUMBER

9. SPONSORING / MONITORING AGENCY NAME(S) AND ADDRESS(ES)
National Aeronautics and Space Administration
Washington, DC 20546-0001

10. SPONSORING / MONITORING AGENCY REPORT NUMBER
NASA TM 107567

11. SUPPLEMENTARY NOTES
Presented at the 33rd AIAA/ASME/ASCE/AHS/ASC Structures, Structural Dynamics and Materials Conference, Dallas, Texas, April 13-15, 1992

12a. DISTRIBUTION / AVAILABILITY STATEMENT
Unclassified-Unlimited
Subject Category 02

12b. DISTRIBUTION CODE

13. ABSTRACT (Maximum 200 words)

Modifications to a three-dimensional, implicit, upwind, unstructured-grid Euler code for aeroelastic analysis of complete aircraft configurations are described. The modifications involve the addition of the structural equations of motion for their simultaneous time integration with the governing flow equations. The paper presents a detailed description of the time-marching aeroelastic procedure and presents comparisons with experimental data to provide an assessment of the capability. Flutter results are shown for an isolated 45° swept-back wing and a supersonic transport configuration with a fuselage, clipped delta wing, and two identical rearward-mounted nacelles. Comparisons between computed and experimental flutter characteristics show good agreement, giving confidence in the accuracy of the aeroelastic capability that was developed.

14. SUBJECT TERMS Aeroelasticity Unsteady Aerodynamics Computational Fluids Dynamics Transonic Aerodynamics	15. NUMBER OF PAGES 12
	16. PRICE CODE A03

17. SECURITY CLASSIFICATION OF REPORT Unclassified	18. SECURITY CLASSIFICATION OF THIS PAGE Unclassified	19. SECURITY CLASSIFICATION OF ABSTRACT Unclassified	20. LIMITATION OF ABSTRACT